Journal of Materials Chemistry C c7tc00486a

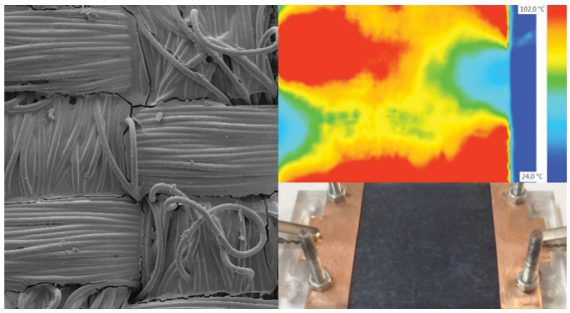

Glycerol/PEDOT:PSS coated woven fabric as a flexible heating element on textiles

Maria R. Moraes, Alexandra C. Alves, Fatih Toptan, Marcos S. Martins, Eliana M. F. Vieira, Antonio J. Paleo, Antonio P. Souto, Washington L. F. dos Santos, Maria F. Esteves and Andrea Zille*

A cost-competitive, flexible and safe thermoelectric polyamide 6,6 (PA66) fabric coated with glycerol-doped PEDOT:PSS (PEDOT:PSS + GLY) for use in large area textiles as a heating element in several applications.

Please check this proof carefully. **Our staff will not read it in detail after you have returned it.**

Translation errors between word-processor files and typesetting systems can occur so the whole proof needs to be read. Please pay particular attention to: tabulated material; equations; numerical data; figures and graphics; and references. If you have not already indicated the corresponding author(s) please mark their name(s) with an asterisk. Please e-mail a list of corrections or the PDF with electronic notes attached – do not change the text within the PDF file or send a revised manuscript. Corrections at this stage should be minor and not involve extensive changes. All corrections must be sent at the same time.

Please bear in mind that minor layout improvements, e.g. in line breaking, table widths and graphic placement, are routinely applied to the final version.

Please note that, in the typefaces we use, an italic vee looks like this: v, and a Greek nu looks like this: ν.

We will publish articles on the web as soon as possible after receiving your corrections; **no late corrections will be made.**

Please return your **final** corrections, where possible within **48 hours** of receipt, by e-mail to: materialsC@rsc.org

Queries for the attention of the authors

Journal: **Journal of Materials Chemistry C**

Paper: **c7tc00486a**

Title: **Glycerol/PEDOT:PSS coated woven fabric as a flexible heating element on textiles**

Editor's queries are marked on your proof like this Q1, Q2, etc. and for your convenience line numbers are indicated like this 5, 10, 15, ...

Please ensure that all queries are answered when returning your proof corrections so that publication of your article is not delayed.

Query reference	Query	Remarks
Q1	For your information: You can cite this article before you receive notification of the page numbers by using the following format: (authors), J. Mater. Chem. C, (year), DOI: 10.1039/c7tc00486a.	
Q2	Please carefully check the spelling of all author names. This is important for the correct indexing and future citation of your article. No late corrections can be made.	
Q3	Do you wish to add an e-mail address for the corresponding author? If so, please supply the e-mail address.	
Q4	The sentence beginning ''A cost-competitive, flexible and...'' has been altered for clarity, please check that the meaning is correct.	
Q5	The sentence beginning ''Samples were scanned...'' has been altered for clarity, please check that the meaning is correct.	
Q6	The sentence beginning ''This set-up allows a...'' has been altered for clarity, please check that the meaning is correct.	
Q7	The sentence beginning ''A reduction of the...'' has been altered for clarity, please check that the meaning is correct.	
Q8	''Temperatura'' appears to be spelled incorrectly in Fig. 3. Please could you supply a corrected version (preferably as a TIF file at 600 dots per inch) with your proof corrections.	
Q9	The caption to Fig. 6 has been altered for clarity, please check that the meaning is correct.	
Q10	The sentence beginning ''These results confirm...'' has been altered for clarity, please check that the meaning is correct.	
Q11	The meaning of the sentence beginning ''Despite only part of the...'' is not clear – please provide alternative text.	
Q12	Ref. 35: Please provide the initial(s) for the 2nd author.	
Q13	Ref. 78: Please provide the full list of author names (including initials).	

Journal of Materials Chemistry C

PAPER

Glycerol/PEDOT:PSS coated woven fabric as a flexible heating element on textiles†

Cite this: DOI: 10.1039/c7tc00486a

Maria R. Moraes,[a] Alexandra C. Alves,[b] Fatih Toptan,[bc] Marcos S. Martins,[b] Eliana M. F. Vieira,[b] Antonio J. Paleo,[a] Antonio P. Souto,[a] Washington L. F. dos Santos,[d] Maria F. Esteves[a] and Andrea Zille *[a]

A polyamide 6,6 (PA66) fabric pre-treated with a double barrier dielectric (DBD) atmospheric plasma in air was coated with 1 and 5 layers of an intrinsically conducting glycerol-doped PEDOT:PSS polymer (PEDOT:PSS + GLY) with the final objective of developing a cost-competitive and temperature controllable flexible-heating element to be used in clothing encapsulated between an outer and an inner separator layer in order to provide heat-reflecting properties and uniform temperature distribution, respectively. FTIR, DSC, TGA, SEM, EDS, XRD and DMA analyses show significant changes in morphology, chemistry, enthalpy, crystallinity and glass transition temperature confirming that PEDOT:PSS and glycerol are not only spread over the PA66 yarn surfaces but are dispersed in the bulk facilitating relaxation and increasing structure and chain flexibility. Electrochemical and electrical resistivity (ρ) measurements confirm that the plasma treated PA66 coated with 5 layers of PEDOT:PSS + GLY presents the highest stability, resistance and capacitive behaviour, and the best capability of storing electrical energy. This configuration needs only 7.5 V to induce a temperature change up to 38 °C at a current density of 0.3 A g^{-1}. The desired temperature is easily adjustable as a function of the applied voltage and by the number of coated layers of PEDOT:PSS + GLY. Despite the need to improve the uniformity of the coating thickness on the fabric for uniform heat generation, the observed results are quite impressive since they can be compared to the temperature obtained in carbon nanotube composites using similar voltages. This cost-competitive, safe, highly flexible and stable thermoelectric fabric has potential for use in large area textiles as a heating element in a wide range of applications such as garments, carpets, blankets and automotive seats.

Received 30th January 2017,
Accepted 23rd March 2017

DOI: 10.1039/c7tc00486a

rsc.li/materials-c

Introduction

In recent years, the integration of electronic components in a textile substrate, the so-called e-textiles, and the development of textile fibres and yarns of high conductivity has become a new paradigm in the area of smart fibres and fabrics making a whole new range of applications possible.[1,2] The higher flexibility and wear resistance of textiles compared to plastics and papers allow a wide variety of novel wearable applications such as strain sensors,[3] ECG measurement,[4] electrostatic discharge (ESD) protection,[5] motion capture devices,[6] pressure sensors,[7] electromagnetic interference (EMI) shielding,[8] photovoltaic devices,[9] energy storage,[10] supercapacitors,[11] and cooling and heating elements.[12] Initially, the use of traditional pure metal wires for interconnections or metal coatings has been demonstrated to be effective. However, they make devices very heavy, rigid, uncomfortable, costly and ultimately inappropriate for textile integration.[13] Moreover, metal coatings on textiles are subjected to cracking and peeling under bending and abrasion. On the other hand, textile fibres and yarns are known for their light weight, porosity, high surface area and other properties, which perfectly meet the requirements for acting as flexible interconnections when properly treated.[14] Electrical conductivity in textiles may be achieved by direct coating or printing of a conductive polymer composite or by *in situ* polymerization of conjugated polymer systems onto the textile fibre surface.[15] Conducting organic polymers such as polypyrrole,

[a] *2C2T – Centro de Ciência e Tecnologia Têxtil, Universidade do Minho, Campus de Azurém, 4800-058 Guimarães, Portugal*
[b] *CMEMS-UMinho – Center for MicroElectromechanical Systems, Universidade do Minho, Campus de Azurém, 4800-058 Guimarães, Portugal*
[c] *Departamento de Engenharia Mecânica, Universidade do Minho, Campus de Azurém, 4800-058 Guimarães, Portugal*
[d] *Departamento de Engenharia Têxtil, Universidade Estadual de Maringá, Av. Reitor Zeferino Vaz, s/n, Campus Universitário, C.P. 171, 87360-000, Goioerê-Paraná, Brazil*

† Electronic supplementary information (ESI) available: Additional information about the set-up of the electrochemical cell and Joule heating experiments. SEM and EDS images of the plasma treated polyamide 6,6. Additional discussion, XRD and SEM about the effect of the temperature on the current drop at high voltages. See DOI: 10.1039/c7tc00486a

polyaniline and poly(3,4-ethylenedioxythiophene) doped with poly(styrene sulfonate) (PEDOT:PSS) have been studied to realize flexible devices for organic solar cells, printed electronic circuits, organic light-emitting diodes, actuators, electrochromic devices, supercapacitors, and biosensors without the use of inorganic materials.[16–18] Conducting organic polymers, because of their lightweight, relatively high conductivity, stability, and flexibility, are particularly well-suited for the fabrication of conductive textiles.[19] Different coating techniques such as physical evaporation and plasma-enhanced and thermally-initiated CVD have already been exploited for developing uniform layers of conductive polymers on the fibre surface. However, fibres coated with conductive polymers are usually produced by a simple dip coating technique and subjected to drying and annealing for film formation.[20] In this fashion, the polymer can eventually enter into the fibre structure allowing a higher volume of intrinsically conductive material.[21] PEDOT:PSS is one of the most extensively explored conducting organic polymers for use in thin-film conductive coatings due to its stability, high conductivity and solution processability.[22] PEDOT is a stable conjugated polymer, which remains oxidized, highly conductive, and water dispersible in a complex with PSS.[15] PEDOT:PSS water dispersions are commercially available and used predominantly in electronic devices, electrodes in electroluminescent displays, LED's, antistatic coating and organic solar cells.[23] Commercially available PEDOT-coated textile fibres such as nylon, PET and viscose are already available showing improved mechanical and electrically conductive properties.[24] Moreover, several studies demonstrate the feasibility of PEDOT:PSS based textiles for antistatic finishing, electromagnetic shielding or biomechanical monitoring.[25–27] Recently, the conductivity of PEDOT-PSS films has been discovered to be enhanced by about two or three orders of magnitude by adding multiple polar organic polymers, co-solvent systems, zwitterionic surfactants, acids, polyalcohols or high-boiling-point solvents such as dichloroacetic acid, poly(vinylpyrrolidone), dimethyl sulfoxide (DMSO), glycerol, sorbitol and ethylene glycol.[28–30] The mechanism of the conductivity enhancement of these compounds is still unclear. However, the most acknowledged model suggests that these additives cause a rearrangement in the morphology of the polymers upon drying, increasing the phase separation between the insulating PSS and the conducting PEDOT.[31,32] The most impressive results have been obtained using PEDOT:PSS doped with polyalcohols such as sorbitol or glycerol because there is no change in optical transparency. On the contrary, conventional oxidative doping alters the coating optical transmittance in the visible region due to the absorption of radical cations.[33]

Temperature control is one of the most important functions in textiles. Passive heating textiles are traditionally based on the heat-insulating properties of a combination of different layers of fabrics. An alternative concept is the development of clothing that actively generates heat ensuring an improved control over the temperature gradient between the skin and the environment. Active heating textiles are applied in a wide range of fields such as sport, leisure, medicine, the aircraft industry, automotive, heated floors, walls and roofs.[34] The majority of the heating elements are based on Joule's heat principle, according to which heat is generated when an electric current passes through a conductive material.[35] Since the mid 20th century, metallic heating elements, graphite elements, conductive rubber and water heater systems have been used in heated fabrics and personal heating garments such as wearing apparels, blankets and gloves.[36] However, these heating elements are often not appropriate for large-area flexible thermogenerators because of their cost, rigidity, increased mass of clothing, limited abstraction of sweat and the presence of hot spots.[37] Resistive heating fabrics based on fibres coated with conductive polymers such as PEDOT:PSS are able to dissipate the generated temperature more evenly avoiding hot spots and are more appropriate for application near the skin because of thermal safety and higher temperature gradients.[27] However, the literature about conversion of electrical energy into thermal energy in textile fibres coated with PEDOT:PSS is very limited since research is focused on two-dimensional films, paper or on using PEDOT:PSS in conjugation with metals.[38]

The objective of this work was to investigate the chemical and dynamic mechanical behaviour, electrical conductivity and thermoelectric properties of a polyamide 6,6 (PA66) fabric coated with glycerol-doped PEDOT:PSS (PEDOT:PSS + GLY) to be used as a flexible heating element in clothing (winter jacket). The design of the active clothing will be able to ensure an appropriate distribution of temperature on the inner side and at the same time to reduce the heat dispersion on the outer side of the clothing by enclosing the heating element between two different breathable and water resistant separator layers. PA66 fabric, pre-treated with a DBD atmospheric plasma in air to enhance substrate adhesion, was dip-coated in a commercial PEDOT:PSS dispersion doped with glycerol and annealed at 120 °C for 10 minutes. The thermal and dynamic mechanical properties of the coated fabrics were evaluated by DSC analysis, TGA and DMA in order to correlate the structural changes of the fabric with PEDOT:PSS deposition. FTIR, XRD and SEM analyses were performed in order to study the effect of electrical voltage and heat on the coating surface chemistry and morphology. Electrochemical and four-point resistivity measurements have been used to gain further understanding of the influence of the addition of glycerol and of plasma pre-treatment on the PEDOT:PSS coated PA66. The electrical current behaviour was also monitored under tension, bending and torsion strains to evaluate the flexibility and wearability of the conductive textiles. Finally, several electrical voltages were applied at constant electrical current and the generated Joule's heat was evaluated using an infrared camera enabling the measurement of temperature distribution on the surface of the fabrics.

Experimental

Materials

Commercial polyamide 6,6 (PA66) fabric with a warp density of 40 threads cm^{-1}, a weft density of 18 threads cm^{-1} and a weight

per unit area of 135 g m^{-2} was used in this study. The samples were pre-washed with 1% non-ionic detergent at 30 °C for 30 min, then rinsed with water for another 15 min, and finally dried before DBD plasma treatment. A commercial aqueous dispersion of PEDOT:PSS with a PEDOT to PSS ratio of 1 : 2.5 by weight was purchased from Sigma-Aldrich. All other reagents were purchased from Sigma-Aldrich and were of analytical grade and used without further purification.

Plasma treatment

The DBD plasma treatment was conducted in a semi-industrial prototype (Softal Electronics GmbH/University of Minho) working at room temperature and atmospheric pressure, using a system of a metal electrode coated with ceramic and counter electrodes coated with silicon, with 50 cm effective width, the gap distance fixed at 3 mm, and producing discharge at a high voltage of 10 kV and low frequency of 40 kHz. The machine was operated at the optimized parameters: 1 kW power, 4 m min^{-1} velocity, 5 passages corresponding to a dosage of 2.5 kW min m^{-2} (Fig. S6 in ESI†). Plasmatic dosage is defined by eqn (1):

$$\text{Dosage} = \frac{N \cdot P}{v \cdot l} \quad (1)$$

where, N = number of passages, P = power (W), v = velocity (m min^{-1}), and l = width of treatment (0.5 m).

PEDOT:PSS deposition on polyamide

Commercial nylon fabrics with and without plasma treatment were cut into pieces of 10 × 10 cm after being washed and dried. Then, the fabrics were dip-coated in a PEDOT:PSS dispersion with and without 5% w/w of glycerol. Up to 10 layers were tested, however, after 6 layers the fabric starts to become too rigid and bulky. Moreover, for each additional layer the coating becomes more irregular. The five-layer coating was chosen as the limit to maintain the flexibility of the textile fabric as well as a reasonable uniformity of the coating. Two types of fabric samples for each used dispersion were prepared: (i) a fabric dip-coated with a single layer of PEDOT:PSS dispersion and (ii) a fabric dip-coated with 5 layers of PEDOT:PSS dispersion (Fig. S7 in ESI†). After each dip coating, the sample fabrics were annealed at 120 °C for 10 minutes. They were dip-coated under normal lab conditions at 20 °C and 40% relative humidity and, after annealing, dried in air. The mass loading in the fabrics was calculated from the difference in weight before and after coating. Samples were stored in a desiccator and dried in an oven for 30 min at 60 °C before use. All values were averaged over three samples.

Scanning electron microscopy (SEM) and energy dispersive X-ray spectroscopy (EDX)

Morphological analyses and thickness measurements of fabrics were carried out using an ultra-high resolution field emission Gun scanning electron microscope (FEG-SEM), NOVA 200 Nano SEM, FEI Company. Secondary electron images were recorded at an acceleration voltage at 5 kV. Backscattering electron images were collected at an acceleration voltage of 15 kV. Samples were covered with a Au–Pd film (80–20 weight%) in a high-resolution sputter coater, 208HR Cressington Company, coupled with a MTM-20 Cressington high-resolution thickness controller. The atomic composition of the membrane was examined using the energy dispersive spectroscopy (EDS) capability of the SEM equipment using an EDAX Si (Li) detector and an acceleration voltage of 5 kV.

FTIR-attenuated total reflection spectroscopy (FTIR-ATR)

A Nicolet Avatar 360 FTIR spectrophotometer (Madison, USA) with a horizontal attenuated total reflectance (HATR) accessory was used to record the FTIR-ATR spectra of the fabrics, performing 60 scans at a spectral resolution of 16 cm^{-1} over the range 650–4000 cm^{-1}. All measurements were performed in triplicate.

Differential scanning calorimetry (DSC)

The DSC analysis was carried out on a Mettler-Toledo DSC822 instrument (Giessen, Germany). The samples were previously dried at 60 °C for 1 h and placed into an aluminium sample pan. The analysis was carried out in nitrogen atmosphere with a flow rate of 20 mL min^{-1} and heating rate of 10 °C min^{-1}. The DSC trace was obtained in the range 25–300 °C. The heat flow *vs.* temperature graph was plotted.

Thermal gravimetric analysis (TGA)

Thermogravimetric analysis was performed on a Modulated TGA Q500 from TA Instruments. The TGA trace was obtained in the range 40–900 °C under nitrogen atmosphere with a flow rate of 20 mL min^{-1} with a rise of 10 °C min^{-1}. The samples were previously dried at 60 °C for 1 h and placed into a porcelain sample pan. The weight (percentage) *vs.* temperature graph was plotted.

Dynamic mechanical analysis (DMA)

The dynamic mechanical analysis (DMA) experiments were performed using a TRITEC 2000B DMA from Triton Technology (UK) in tension mode. The described values for the compression modulus were collected at a frequency of 1 Hz. The temperature dependence of the storage modulus and loss tangent was measured in the temperature range from 30 to 200 °C at 2 °C min^{-1}.

X-Ray diffraction (XRD)

The crystalline structure of the fabrics was characterized by XRD using a Bruker D8 Discover diffractometer. Samples were scanned using Cu Kα X-ray radiation (λ = 1.541 Å) in $\theta/2\theta$ mode at a step size of 0.04 deg min^{-1} over a 2θ range from 2° to 10° (corresponding to a lattice spacing range between 44.14 and 8.84 Å). The interlayer spacing of the coating was determined using Bragg's law.

Electrochemical tests

Electrochemical tests consisting of electrochemical impedance spectroscopy (EIS) and cyclic voltammetry (CV) were performed in 9 g L^{-1} NaCl electrolyte at room temperature in atmospheric

air using a Gamry Potentiostat/Galvanostat (model Reference–600). A conventional three-electrode electrochemical cell containing 150 mL of electrolyte was used where a saturated calomel electrode (SCE) was used as the reference electrode (RE), a Pt electrode was used as the counter electrode (CE), and the immersed samples having a total exposed area of 6 cm^2 were used as the working electrode (WE). The EIS data acquisition was performed at open circuit potential (OCP) where the OCP was considered stable when ΔE was below 60 mV h^{-1}, by scanning a range of frequencies from 100 kHz to 10^{-1} Hz with 10 points per frequency decade and the amplitude of the sinusoidal signal was selected as 10 mV in order to guarantee linearity of the electrode response. Following EIS, cyclic voltammetry measurements were performed between −0.5 V_{SCE} and 0.4 V_{SCE} at a scanning rate of 1 mV s^{-1}. All tests were repeated at least three times in order to ensure repeatability.

Film thickness

The fabric thickness was measured using a digital micrometer (Mitutoyo, Japan) with an accuracy of 0.5 μm. Ten thickness measurements were taken on each test sample at different, randomly chosen points. The mean value was used to infer the average PEDOT:PSS coating thickness and resistivity.

Resistivity measurements and Joule heating

The electrical resistivity (ρ) of the samples was measured using the conventional four-probe van der Pauw geometry, at room temperature, and using a power generator with D. C. (Yokogawa 7651 programmable DC source) current supplies the electric circuit that includes a multimeter (KeYsight 34410A). Joule effect testes were carried out using samples of 7 × 6 cm assembled between two copper electrodes, gripping the pieces on the extremes of the upper and the lower sides (Fig. S8 in ESI†). The orientation of the fabric piece is determined, according to whether the warp or the weft threads are laid out perpendicularly to the electrodes. A power generator with D. C. (Agilent Technologies, model N5772A, 600 V, 2.6 A, 1560 W) current supplies the electric circuit that includes a multimeter (Agilent Technologies LXI, model 34410A 6 1/2 Digit). The width of the sample was measured between the two external boards of the fabric piece and the relevant length used in the transport of the current corresponds to the gap between the internal boards of the two copper electrodes since the sample surfaces in contact with the electrodes do not take part in the transport of the current because copper is a much better conductor than nylon fabrics. This set-up allows a 6 × 6 cm square of the sample to be measured. The stretching and the pressure exerted on the samples are always constant. The samples were first dried for 24 h at 60 °C in order to desorb the water contained in the pores. For each sample, various electrical voltages were applied (3, 4.5, 6, 7.5, 9, 10.5, 12, 15, 18, 21, 24, 30, 33, 36, 40, 43 V) at a constant current of 2 A for 10 minutes. For each sample, a test of 60 minutes was also performed at a voltage of 12 V. Measurements were carried out at room temperature controlled by a thermo-hygrometer (RH Meter, model R 200). The temperature distribution on the fabric surface was measured using an infrared camera (TESTO 876 model). The thermographs enable the distribution of temperature on the surface of the fabrics to be visualized with a resolution of about 0.1 cm^2. The measurement accuracy was about 0.1 °C. Data were then represented as the average temperature calculated by TESTO software (IRSoft Version 3.8) *versus* applied voltage.

Strain *versus* current

Fabric strain *versus* applied force and time was measured (at 20 °C and 65% RH) on an Instron Universal Testing Machine (Model 4500, Instron Corporation) using a 2.5 kN load cell at a crosshead speed of 1 mm min^{-1}. Samples were tested in the warp and weft directions at the maximum load of 250 N. The current evolution as a function of the applied force was recorded using samples of 6 × 6 cm assembled between two copper electrodes, inserting the pieces on the extremes of the upper and the lower grips (Fig. S9 in ESI†). A power generator with D. C. (Agilent Technologies, model N5772A, 600 V, 2.6 A, 1560 W) current supplies the electric circuit that includes a multimeter (Agilent Technologies LXI, model 34410A 6 1/2 Digit). A test until the breaking point was also performed. Two tests to evaluate the current behaviour under bending and torsion strains were performed. The samples were gripped at the extremes between two copper electrodes. Several cycles (up to 200) of bending (90°) and torsional (180°) strain were applied and the current evolution was recorded. The tests were conducted using a custom-built two-point bending and twisting device.

Results and discussion

FTIR-ATR analysis

The FTIR-ATR spectrum of untreated PA66 (Fig. 1 – Control) showed the characteristic bands of nylon at 3286 cm^{-1}, 2931 cm^{-1} and 2854 cm^{-1} attributed to N–H stretching vibrations, CH_2 asymmetric and symmetric stretching vibrations, respectively. The absorption band at 1620 cm^{-1} was assigned to the amide carbonyl C═O stretching vibration of the secondary amide band (amide I).[39] The amide II band at 1528 cm^{-1} may

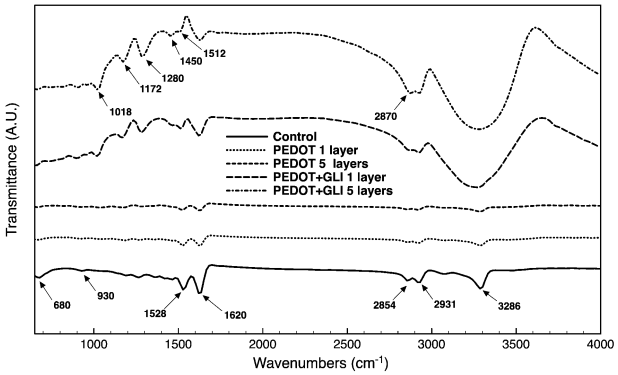

Fig. 1 FTIR-ATR spectra of plasma treated PA66 fabric with 1 and 5 layers of deposited PEDOT:PSS and PEDOT:PSS + 5% w/w of glycerol.

be attributed to N–H bending motion, the band at 930 cm^{-1} to the crystalline peaks of the amide axial deformation C–C═O and the band at 680 cm^{-1} to the bending of the O═C–N group.[40]

After plasma treatment, a slight increase in the intensity and broadening of the C═O stretching band as well as of the bending of the O═C–N group were observed suggesting oxygen addition to the fibre surface.[41,42] After the deposition of PEDOT:PSS, no significant differences can be noted between the sample with and without plasma treatment (Fig. S2 in ESI†), thus only the results with plasma treatment are reported in Fig. 1. The samples with 1 and 5 layers of deposited PEDOT:PSS showed the characteristics peaks of PEDOT but no significant differences can be noted between the two samples. The peaks in the spectrum at 1512 and 1280 cm^{-1} are attributed to the C═C and C–C bonds of the thiophene ring.[43] The peak at 1176 cm^{-1} corresponds to the asymmetric stretching vibrations of the $-SO_3^-$ group of PSS.[44] However, since the C═C stretchings of the phenyl side groups of PEDOT and PSS have vibrations between 1350 and 1600 cm^{-1}, they are hard to distinguish because of the superimposition of the amide carbonyl C═O stretching vibration of polyamide. The introduction of 5% w/w of glycerol in the PEDOT:PSS solution showed remarkable differences in the IR spectra of the coated fabric with the growth of bands in the 800–1500 cm^{-1} region typical of doped PEDOT. Especially, the appearance of a peak at 1450 cm^{-1} indicates that the density of Cα═Cβ in the PEDOT rings has increased, which is beneficial to obtain a low-resistance coating.[45] The broad peaks around 3200 and 2800 cm^{-1} are due to the O–H and C–H stretching vibrational modes of G-, respectively, and indicate that the annealing process at 120 °C does not degrade the glycerol moieties in the coating.[46]

The persistence of these broader peaks and the shift of stretching vibrational modes at around 2800 cm^{-1} as well as the intensification of the peaks in the region between 800 and 1500 cm^{-1} indicate interactions between the O–H group of glycerol and the SO_3^- group of PSS.[47] This suggests that the addition of glycerol could lead to a structural reorientation of PEDOT:PSS chains that could increase coating stability, intensify the number of electrostatic pairing events and promote subtle changes in the molecular ordering of the PEDOT units, which could be responsible for the increased conductivity of the blend.[30,48] The surface sheet resistance of the PEDOT:PSS + GLY coated fabric is greatly affected by the annealing conditions of the conducting coating. Higher current density has been observed using annealing temperatures close to the boiling point of glycerol (170 °C).[46] However, due to the temperature-sensitive nature of textiles it is not possible to use a higher curing temperature than 120 °C in this case.

After the chemical characterization of the PEDOT:PSS coating, one of the main objectives of the present research is to evaluate the effect of the deposition of the conductive polymer on the thermo-mechanical behaviour of the polyamide fabric. The most commonly used thermal analysis techniques for the studies of textiles are DSC, TGA, and DMA. Since textiles are thermal sensitive materials, when heated they can lose their main features. Thus, attesting their stability is highly required for wearability. Moreover, it is important to characterize the thermal and mechanical properties of textiles in order to optimize the processing conditions, for defect analysis and for quality assurance purposes. TGA gives important information about fibre degradation indicating the temperature at which mass loss starts and also provides unique features at the molecular level of the analysed material. DSC allows rapid detection and measurement of the physical and chemical transformations that a material undergoes when subjected to heating. DMA is the most sensitive technique for the measurement of the glass transition and for the detection of secondary relaxation events that are not detectable by other thermal analysis techniques resulting in vital fabric mechanical information such as impact resistance and toughness.

DSC analysis

DSC analysis of the second heating confirms the PEDOT:PSS amorphous nature (Fig. 2). No glass transition peaks were observed below the range of thermal degradation due to the strong ionic bonding interaction between PEDOT and PSS.[49] Since plasma treatment can lead to surface alteration without

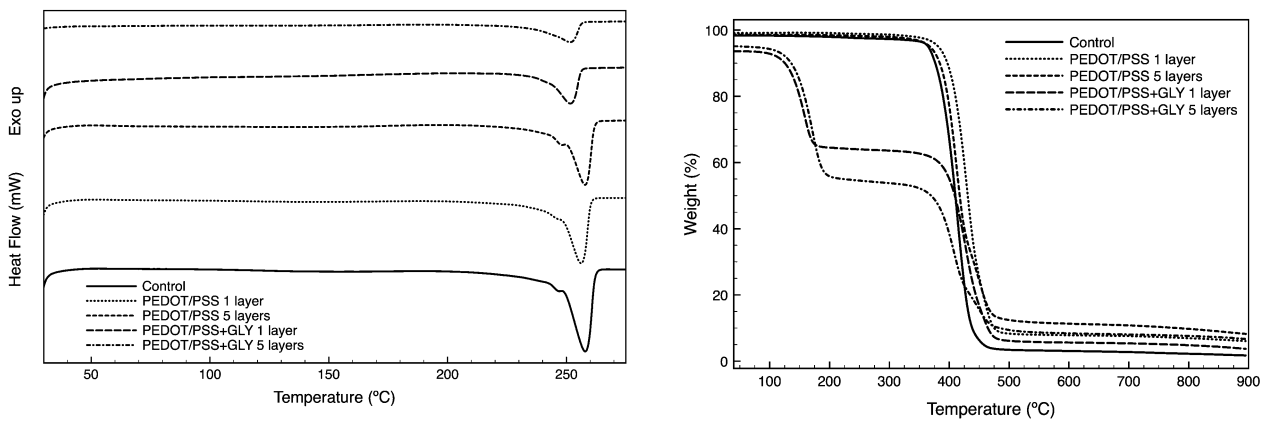

Fig. 2 Differential scanning calorimetry (DSC) and thermogravimetric (TGA) analyses of plasma treated PA66 fabric with 1 and 5 layers of deposited PEDOT:PSS and PEDOT:PSS + 5% w/w of glycerol.

Table 1 Main DSC thermal transitions, TGA weight loss temperature, residual weight and crystallinity of plasma treated fabrics

	Crystallinity (%)	ΔH (J g^{-1})	T_m (°C)	T peaks of 1st derivative (°C)	Residual weight (%)
Polyamide 6,6	36.7	72.3	257.7	413.5	3.4
PEDOT:PSS 1 layer	29.4	57.8	256.0	431.5; 462.2	7.0
PEDOT:PSS 5 layers	29.8	58.6	257.6	411.0; 449.4	9.2
PEDOT:PSS + GLY 1 layer	18.5	36.4	251.4	159.8; 426.1; 460.1	10.1
PEDOT:PSS + GLY 5 layers	13.8	27.1	251.8	173.1; 409.3; 450.4	11.6

modifying the bulk properties of the materials, as expected, no significant differences between untreated and plasma treated samples can be depicted in the DSC thermograms (Fig. S2 in ESI†).[50] Both pure and coated PA66 showed a broad endothermic peak at ~255 °C, indicating the melting of α-crystals[51] and a smaller endothermic peak at ~245 °C which is more noticeable in the control PA66 and in the PEDOT:PSS samples without glycerol (Table 1). The presence of multiple fusion endotherms in the case of semi-crystalline PA66 is not new and has been a subject of extensive contradictory interpretations. Several hypotheses have been proposed about the melting behaviour of PA66 including the effects due to orientation, the presence of two different crystals distributions, the presence of triclinic and pseudo-hexagonal crystalline phases and melting of different crystal structures including the α, β and γ forms.[52,53] However, no crystalline transition can be observed in the XRD patterns of the PA66 composites and the two observed peaks corresponding to the α crystal planes with no evidence of the presence of the β phase peak (Fig. S4 in ESI†). Moreover, in PA66 the α-β Brill transition temperature occurs between 170 °C and 220 °C, well below the melting temperature which is in the range of 250 °C to 272 °C.[54,55] Therefore, this suggests that only one crystal structure with two different populations of thickness is responsible for the presence of two peaks during the melting process of PA66.[56] The peak at the lower temperature seems to originate from the melting of thinner crystallites, which in turn could recrystallize into thicker crystallites.[57] The PEDOT:PSS coated PA66 fabrics show a slight decrease in melting point but a significant decrease in both enthalpy and crystallinity. The PA66 fabrics coated with 1 and 5 layers of PEDOT:PSS display a similar crystallinity around 29%, which is almost 19% lower than the 36.7% crystallinity of the pure PA66 (calculated based on 100% crystalline PA66 with an enthalpy of 197 J g^{-1}). The deposition of PEDOT:PSS on PA66 decreases the melting enthalpy to an average of 58 J g^{-1} from the value of 72 J g^{-1} of pure PA66. After the introduction of glycerol in the coating system, a further decrease in enthalpy and crystallinity as well as in the melting point was observed. The 1-layer coating with PEDOT:PSS + GLY displays a 50% reduction in crystallinity, while the 5-layer coating shows a 62% reduction clearly due to the presence of a higher amount of glycerol in the coated material. The peak height of the enthalpies drops to 36 and 27 J g^{-1} for PA66 coated with 1 and 5 layers of PEDOT:PSS + GLY, respectively. A reduction of the melting temperature of about 6 °C is recognizable for PA66 coated with 1 and 5 layers of PEDOT:PSS + GLY with a concomitant disappearance of the second small endothermic peak in the DSC thermogram. It was previously suggested that the addition of glycerol or other polyalcohols could change the chemical structure of PEDOT:PSS, increasing the number of polarons and density of the carriers.[58] Moreover, the small glycerol molecules in the PEDOT:PSS moiety could diffuse easily on the surface of the yarns resulting in an enhanced plasticization of the fibres with lower melting points, enthalpy and crystallinity than pure semi-crystalline PA66. The main factors affecting polymer enthalpy and crystallinity are the inclusion of intermolecular bonding as well as an increase in structure and chain flexibility.[59] The melting point decrease seems to indicate that the PEDOT:PSS + GLY moiety significantly decreases the backbone rigidity with the formation of a complex system that influences the thermal parameters of the PEDOT:PSS + GLY coated PA66 fabric. The decrease in the enthalpy of fusion and crystallinity confirms an interaction between PEDOT:PSS and glycerol because of the presence of –OH groups capable of hydrogen bonding as well as a change in the characteristic of the treated PA66 fibres.[60] These changes are important in terms of fabric application in garments since a lower melting point could limit the operational temperature range of the heating elements. Moreover, the enhanced plasticization of the fibres due to glycerol addition should be carefully assessed when rigidity of the system is required because glycerol absorbs moisture and could considerably decrease the properties of the composite.

TGA

Thermogravimetric curves (Fig. 2) at a heating rate of 10 °C min^{-1} showed that the degradation of the PA66 control sample takes place in a well-defined single step due to a random chain scission process between 350 and 460 °C with a derivative thermogravimetric (DTG) temperature peak of 413.5 °C (Table 1).[61] Above this temperature, the weight remains constant until 900 °C leading to a small residue content of 3.4%. The thermal degradation of PA66 coated with 1 and 5 layers of PEDOT:PSS did not apparently show significant differences compared with the control curve in accordance with the DSC data (Fig. 2). However, the DTG analysis reveals a two-stage degradation with the appearance of shoulder peaks in the curves (data not shown). PA66 coated with 1 layer of PEDOT:PSS displays a DTG peak at 432 °C and a small shoulder at 462 °C, while PA66 coated with 5 layers of PEDOT:PSS shows a peak at 411 °C and a noticeable shoulder at 449 °C.

The weight loss observed in the temperature range of 365–435 °C could be attributable to the superimposing PA66 and thiophene main chain decompositions and in the range of 435–550 °C to the aromatic thiophene and phenyl groups.[62] The more PEDOT:PSS is coated on the PA66 fabric, the more char is produced and the more noticeable the peak attributable to the

aromatic groups is. The addition of glycerol in the system showed that the degradation takes place in three well-differentiated steps. In the first step, the thermograms showed a fast and significant initial degradation mainly attributed to the evaporation of glycerol between 100 and 200 °C with a 30% and 40% weight loss for 1 and 5 layers of PEDOT:PSS + GLY, respectively.[63] Above this temperature, the weight remains constant until a second and third phase at the same DTG peak temperatures as discussed earlier. A higher solid residue content at 900 °C was observed for 1 and 5 layers of PEDOT:PSS + GLY (~10 and 12%, respectively). These results confirm the presence of both glycerol and PEDOT:PSS in the composite material after the curing of the samples, as confirmed by FTIR analysis. Moreover, the increase in weight percentage corresponding to the residual amount of degradation products still present at 900 °C indicates a higher amount of coated PEDOT:PSS when mixed with glycerol compared with PEDOT:PSS alone. The TGA provides important information regarding the maximum temperature that the textile-heating element can withstand. The addition of glycerol clearly limits the temperature to 100 °C. At this temperature, the glycerol on the coated fabric starts to degrade compromising the electric conductivity of the system. It is clear that the heating element developed in this work cannot be exploited for high temperature applications. In the case of textile applications that require higher temperatures, the coating without glycerol should be considered since it can endure up to 400 °C without significant degradation.

DMA

The dynamic mechanical thermal parameters including tan delta and storage modulus provide important information about the stiffness of the polymer, molecular motion, relaxation process, structural hetero groups, and morphology of the polymer blend systems.[59] Fig. 3 shows that after deposition of 1 and 5 layers of PEDOT:PSS onto the nylon fabric, the storage modulus at 35 °C compared with 0.16 GPa in pure PA66 has increased to 0.21 GPa and 0.25 GPa, respectively, which is an increase of 31% and 36%. Beyond 35 °C, the storage modulus of PA66 with 5 layers of PEDOT:PSS was found to be increased, and a storage modulus peak (0.26 GPa) was observed at 50 °C. This behaviour can be attributed to altered intermolecular bonding that hinders the mobility of the polymer chains at the interfaces due to the higher amount of PEDOT:PSS deposited on the PA66 surface.[64] Differently, PA66 with 1 layer of PEDOT:PSS performs similar to pristine PA66, decreasing the storage modulus with the rise in temperature. The mechanical strength of PEDOT:PSS is attributed to the strong ionic bonding interaction between PEDOT and PSS and to the hydrogen bonds between inter- and intra-molecular PSS chains. Since the modification of the PEDOT chains is not temperature dependent, the amount of water absorbed by the PSS chains in the 5-layer deposition seems to play an important role in determining the final mechanical behaviours of the composite.[65] Different from the DSC analysis, the evolution of the storage modulus and the damping factor (Fig. 3), showed only the α relaxation processes corresponding to the T_g of the PA66 fabrics since PEDOT:PSS does not have a well-defined glass transition value. In addition to the storage modulus increase, the deposition of PEDOT:PSS onto PA66 fabric reduces T_g probably due to the higher loss factor of PEDOT:PSS than PA66. The glass transition temperature of the fabrics was estimated as a peak in the tan δ curve, which corresponds to a sharp decrease in the storage modulus.

The control PA66 displays a T_g of 75 °C, while PA66 coated with 1 and 5 layers of PEDOT showed a similar T_g of 65 and 67 °C, respectively. PEDOT:PSS/PA66 composites display a reduced T_g and improved storage moduli both in the glassy and rubbery regions compared with pristine PA66. The increase in the storage modulus along with the reduction in T_g indicates that PEDOT:PSS acted as an antiplasticizer in PA66. Antiplasticization is defined as a decrease in the glass transition temperature with a simultaneous increase in the stiffness of the polymer matrix by the addition of particular substances.[66] This could be attributed both to the decrease in the free volume in the polymer matrix induced by antiplasticizer shrinkage due to water vapour desorption[67] and by the existence of hydrogen bonding between the antiplasticizer and the polymer.[68,69] These results suggests that PEDOT:PSS is not only spread over

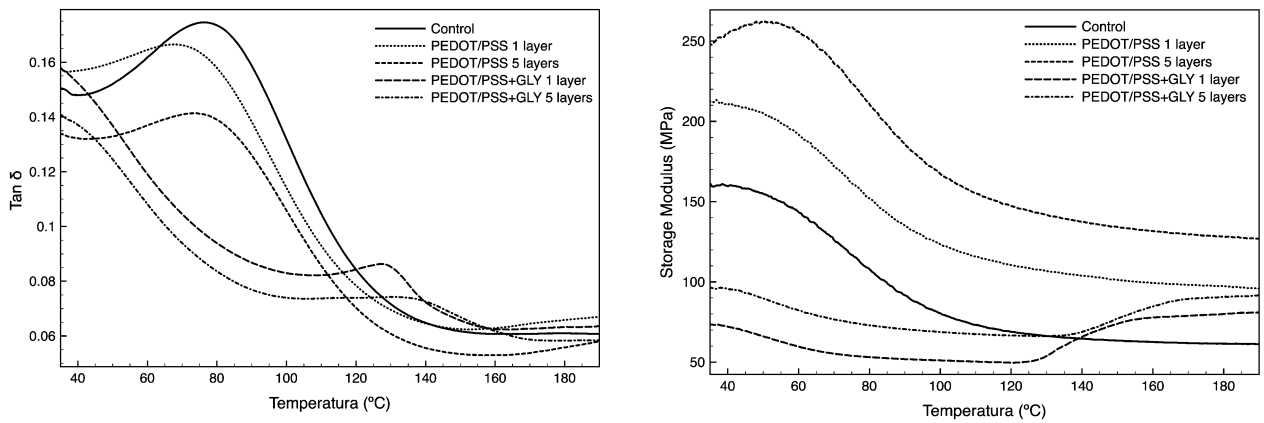

Fig. 3 DMA (storage modulus and damping factor) of the plasma treated PA66 fabric with 1 and 5 layers of deposited PEDOT:PSS and PEDOT:PSS + 5% w/w of glycerol.

the yarn surfaces but could also be dispersed in the bulk PA66 facilitating relaxation.[68]

The addition of glycerol to the system leads to a significant decrease of the storage modulus. Fig. 3 shows that after inclusion of glycerol into PEDOT:PSS, the storage modulus at 35 °C compared with 0.16 GPa in pure PA66 decreases significantly to 0.074 GPa and 0.098 GPa for the 1-layer and 5-layer coatings, which is a decrease of 46% and 61%, respectively. Beyond 35 °C, the storage modulus of the PA66 fabric with PEDOT:PSS + GLY was found to decrease up to 120 °C. After this temperature, the storage modulus starts to increase progressively. This was due to the fact that the glycerol impregnation enhances the swollen state of the PA66/PEDOT:PSS composite and promotes molecular mobility of the chain segments. As a result, the rigidity of the material is decreased. The decrease in the magnitude of tan δ between 35 and 100 °C upon addition of PEDOT:PSS + GLY to the PA66 fibres suggests a good interfacial adhesion between the fibres and the coating. The reason for this behaviour may be attributed to the limited mobility of polymeric chains because of the interactions between the fibre and matrix that cause a decrease in damping factor.[70] The glass transition temperature is clearly shifted to a lower temperature when glycerol is added, also confirming its plasticizing effect on the polymeric network.[71] As seen in Fig. 3, one peak appeared in the tan δ curve between 130 and 140 °C for all samples with glycerol, indicating a transition of the relaxation process of the material.[72] The DMA results reveal that there is an increase in the stiffness of the polyamide fibres, once coated with PEDOT:PSS, while the plasticizing effect of glycerol increases fibre ductility. These results should be taken into consideration in cases where the textile heating element has to be used for applications requiring higher resistance to impact.

Electrical and electrochemical behaviour

In order to understand the contribution of the addition of glycerol and/or plasma treatment on the conducting properties of the different PEDOT:PSS coated samples, the electrical resistivity (ρ) in the dry state was measured. The collected data have shown that, macroscopically, the films were electrically homogeneous. Moreover, the ρ values, measured when applying a constant current in both the warp and weft directions, do not change significantly showing that there is no preferable path for charge movement. It is clear from Table 2 that in the PEDOT:PSS samples without glycerol, ρ displays the lowest values for the 5-layer coating and when plasma is not applied as pre-treatment. Differently, in the case of G-PEDOT:PSS the plasma pre-treated samples showed the lowest value of ρ when plasma was applied but the differences among the applied layers are not as dramatic as those obtained without glycerol. In any case, the average decrease in ρ provided by glycerol addition was one order of magnitude (10 times more efficient). The effect of plasma on PEDOT:PSS conductivity after deposition could be explained by the plasma induced chemical and morphological changes on the fibre surface. Plasma surface pre-treatment introduces oxygen atoms and alters the surface topology by etching in the form of ripple-like structures of submicron size.[73] Plasma treatment of electrodes is routinely performed in order to improve their wetting properties before PEDOT:PSS solution deposition.[74,75] The hydrophilic groups on the plasma-treated surface and the effective dispersant nature of PEDOT:PSS ensure strong bonding by π–π interaction and electrostatic attraction between PEDOT chains and the polymer.[76] However, the highly active oxide surface sites, such as peroxide radicals, induced by plasma treatment seem to act as electron acceptors reducing free electrons at the PA66 interface. This could explain the higher ρ observed after plasma treatment. The addition of five layers of PEDOT:PSS reduces this effect that seems to occur only at the interface between PA66 and the first layer of PEDOT:PSS.[77] Besides the extreme increase in conductivity due to decreased humidity in PEDOT:PSS, the addition of glycerol to the system seems to reverse the plasma effect.[78] Moreover, since plasma greatly improves PEDOT:PSS adhesion, local strains at the interface could fracture the PEDOT:PSS film destroying electrical contiguity and, therefore increasing the resistivity.

The addition of glycerol to the system allows PEDOT:PSS grains to reorient in the direction of the strain easily enduring tensile deformation and improving uniform electrical conductivity.[79]

As stated above, the use of plasma treatment to improve adhesion of PEDOT:PSS is widely reported in the literature. However, this work introduces four main novelties: (i) the plasma assisted deposition of PEDOT:PSS was performed on textiles, while most of the literature reports metals, silica, glass or smooth polymeric sheets as substrates; (ii) atmospheric DBD plasma in air has never been used before to improve the deposition of PEDOT:PSS on textiles; (iii) the plasma deposition in this treatment does not require any expensive carrier gas, cryogenic coil or vacuum pumping system and (iv) this plasma technology allows continuous and uniform processing of very large fabric surfaces.[80] The effect of DBD atmospheric plasma in air on polyamide 6,6 was previously studied by Zille *et al.* DBD atmospheric pressure plasma treatment promotes polyamide

Table 2 Electric resistivity (ρ) and total impedance ($|Z|$) of PA66 coated with 1 and 5 layers of PEDOT:PSS with and without glycerol and plasma pre-treatment

	Volume ρ (Ωm)		$\|Z\|$ (Ω)	
	1 layer	5 layers	1 layer	1 layer
PEDOT:PSS	14.15 ± 5.42	3.21 ± 0.28	1817 ± 823	1817 ± 823
PEDOT:PSS Plasma	30.36 ± 5.59	4.38 ± 0.33	2255 ± 119	2255 ± 119
PEDOT:PSS + GLY	1.30 ± 0.49	0.25 ± 0.07	740 ± 112	740 ± 112
PEDOT:PSS + GLY Plasma	0.22 ± 0.05	0.14 ± 0.03	779 ± 115	779 ± 115

6,6 fibre etching and induces the increase of fibre surface roughness and hydrophilicity-dependent properties through the formation of reactive species producing new functional groups on the polymer surface.[73] DBD plasma-formed reactive species preferentially break the C–N bonds of polyamide, increasing the concentration of polar groups mainly due to the incorporation of oxygen atoms near the surface of the fabric.[81] In a similar fashion as the dyes used in the previous publication, the acidic character of the newly formed small molecules can improve the diffusion inside the fibres allowing PEDOT:PSS to react with the new bonds in the broken chains as well as with the exposed PA66 chain below.[82] These plasma generated low-molecular weight aliphatic chains tend, by oxidation, to form acidic and partially soluble species and may act as a sort of PEDOT:PSS "carrier" into the fibre resulting in widespread and even deposition on the surface and also deep into the interior of the fibres.[81]

To evaluate the electrochemical performance of the system, cyclic voltammetry (CV) and electrochemical impedance spectroscopy (EIS) tests were performed in 9 g L^{-1} NaCl (Fig. S1 in ESI†). Fig. 4 presents the cyclic voltammograms of the 1-layer and 5-layer samples. It has been reported that CV curves presenting an almost rectangular cyclic behaviour indicate some typical capacitor-like characteristics.[83–86] From 1 layer to 5 layers, the peak currents were decreased and the shape of the curves tended to be closer to the shape of an ideal capacitor on all samples except for PEDOT:PSS plasma, indicating a better behaviour as a capacitor. Within the same group of samples (1 layer or 5 layers), the addition of glycerol to PEDOT:PSS always resulted in a decreased resistance (*i.e.* increased slope of the CV curves).[87] On the other hand, the plasma treatment resulted in an increased resistance on the 1-layer samples, whereas no significant differences were observed on the 5-layer samples. This is an expected behaviour since the plasma treatment is expected to directly influence only the first layer of PEDOT:PSS that is directly in contact with the plasma modified PA66 surface.

In addition to the CV measurements, EIS was also performed in order to gain a better understanding of the electrochemical behaviour of the 1-layer and 5-layer surfaces. Fig. 5 shows the EIS spectra of 1-layer and 5-layer samples in the form of Bode diagrams. The lower values observed for $|Z|$ in the high frequency range (10^2 Hz to 10^5 Hz) correspond to the response of the electrolyte resistance.

On the other hand, in the low and middle frequency ranges, the higher values of $|Z|_{f\to 0}$ correspond to the electrochemical resistance of the textile samples. EIS is a sensitive technique using very small signals not influencing the properties of the samples. Among a variety of fields, EIS is also being used for electrochemical characterization of organic coatings.[88] When the $|Z|$ values of the 1-layer and 5-layer samples were compared, no significant differences were observed; however, in accordance with the CV measurements, the addition of glycerol resulted in lower $|Z|$ values for any number of layers (Table 2). It is important to highlight that the applied electrochemical techniques, namely CV and EIS, are surface-sensitive techniques. Thus, as one may expect, the effect of the plasma pre-treatment was only distinguishable on the first layer of the PEDOT:PSS samples which presented a more electrochemically-stable performance. For this reason, SEM–EDS analysis and Joule heating tests were performed only on the plasma treated samples.

SEM and EDS

The surface coverage and morphology of the PEDOT:PSS coating onto PA66 fabric are important for determining the resultant performance. The SEM images of the plasma treated control PA66 fibre (Fig. 6A and Fig. S2, in ESI†) show that the topography of the fibre was uniformly altered after plasma treatment in the form of ripple-like structures of sub-micron size that were induced by plasma etching, as previously observed.[89] Energetic and highly reactive plasma species attacked the fibre surface promoting fibre ablation and

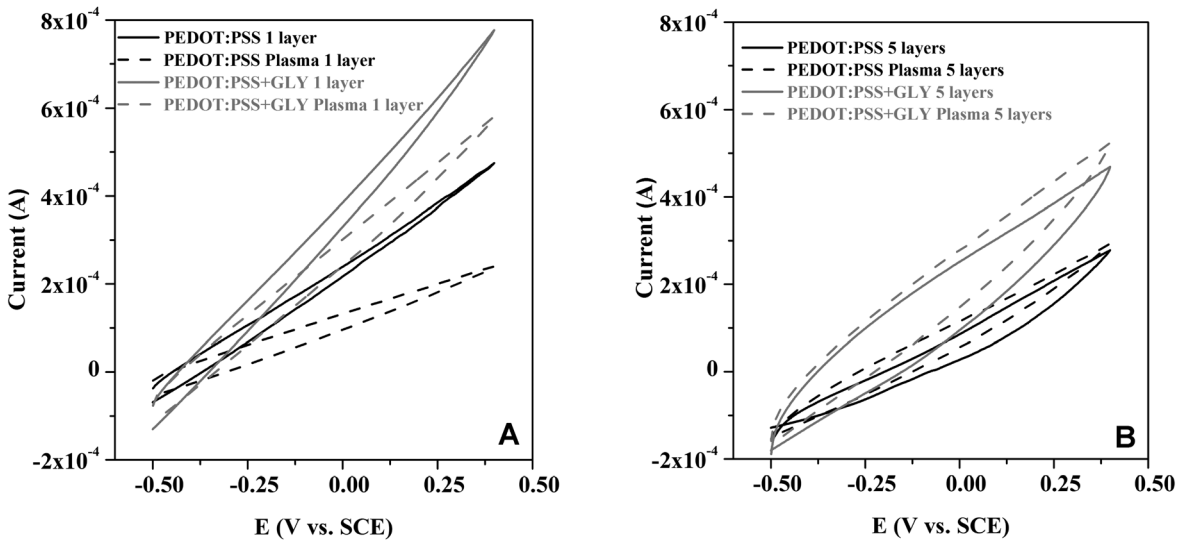

Fig. 4 Cyclic voltammograms of 1-layer (A) and 5-layer (B) samples.

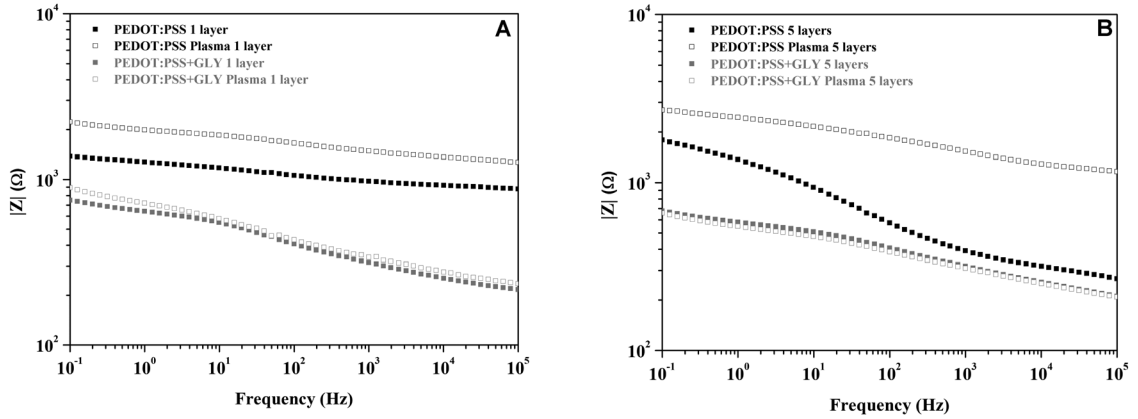

Fig. 5 EIS spectra of 1-layer (A) and 5-layer (B) samples in the form of Bode diagrams.

inducing an increase of the fibre surface roughness and hydrophilicity-dependent properties. Fig. 6 shows the top-view SEM images of PA66 fabric before (Fig. 6A) and after the PEDOT:PSS coating treatment. The coated fabrics with 1 layer of PEDOT:PSS showed an even and smooth covering of the fibre surface which led to the absence of the original surface morphology (Fig. 6B). Furthermore, with an increase in the number of deposited layers the assembled composite multilayer film was visibly detected and smoothly covered the entire fabric surface, revealing a successful coating process (Fig. 6C). The coated fabrics maintained flexibility being able to easily bend and twist but could not retain the softness of the PA66 fabric. After repeated bending, the coating deposited on the PA66 fabric seems to be damaged displaying several cracks especially at the interlaced gap between warp and weft yarns.

Despite cracks being uniformly diffused on the entire fabric surface, the electrical conductivity was not compromised. The introduction of glycerol in the system reduces the cracks on the coated surface as well as their depth due to the plasticizing effect of the polyol (Fig. 6D and E). Moreover, glycerol seems to enhance the amount of PEDOT:PSS deposited onto the PA66 surface with some fibres being completely covered by an even coating. The formation of a uniform PEDOT:PSS coating on the PA66 fibres was verified by the EDS spectra showing C, O and S with their atomic percentages in agreement with the theoretically expected atomic composition of the polymer (Table 3).[90]

The EDS spectrum of the PEDOT:PSS coated fabric indicates that element S evenly covered the coated area suggesting the uniform coverage of the PEDOT:PSS coating on the fabric (Table 3 – *Z*1; Fig. S3 in ESI†).

The total thickness of the coated fabrics was evaluated using a digital micrometer with an accuracy of 0.5 micron. However, the SEM analysis of the coating of PEDOT:PSS was performed in order to confirm the additive effect of the deposited layers. The thickness of 1 layer of coated PEDOT:PSS is about 0.5 μm (Fig. 6F) and the 5-layer coating achieved by layer-by-layer stacking of PEDOT:PSS shows a total thickness of about 2.5 μm (Fig. 6G) confirming that each layer of PEDOT:PSS has an average thickness of 0.5 μm. The 5-layer coated PA66 showed the presence of PEDOT microcrystals on the coating surface (Fig. 6H) with higher sulphur and lower oxygen contents (Table 3 – *Z*2) than the surrounding PEDOT:PSS coating (Table 3 – *Z*1). Usually, the strong electrostatic coupling of entangled PSS inhibits the crystallization of PEDOT.

Thus, PEDOT does not form crystals in the core region of the micelle in the water dispersion even after addition of co-solvents. However, the formation of crystals during solid film fabrication processes at the moment of evaporation of water has been previously reported.[91,92]

Thermoelectric effect

Fig. 7(A) shows the current density as a function of the applied voltage of the plasma treated PEDOT:PSS samples with and without glycerol doping. The current values across all fabrics were measured for 10 min when the voltage was varied from 1 to 12 V. For each selected voltage, the current in the samples stabilized after a few seconds and the resistance remained constant throughout the period of 10 min, with no change in conductivity. All the configurations display a linear behaviour and clearly indicate that the system performance is greatly improved by about 100 times when the polymer is doped with glycerol and the fabric coated with five layers of polymer. The addition of glycerol to PEDOT:PSS significantly reduces the operating voltage allowing conducting fabrics to sustain higher current density. The most endorsed theory about the improvement of conductivity of PEDOT:PSS + GLY is ascribed to the plasticizing effect of glycerol that induces a rearrangement of the PEDOT chains to form better connections among the amorphous PSS.[31,32] The increased interchain interaction and the proposed conformational changes facilitate charge hopping among the conductive PEDOT chains leading to a lower energy barrier and a longer localization length of the charge.[93] Since the generated current of the undoped coated fabric is practically nominal at any tested voltage, the Joule heating experiments were only performed on the PEDOT:PSS + GLY coated fabrics. The temperature response of the plasma-treated PA66 fabrics coated with PEDOT:PSS + GLY to different applied voltages at a current of 2 A is plotted in Fig. 7B. A quasi-exponential increase of temperature with voltage can be observed in both curves. However, because Joule heating is

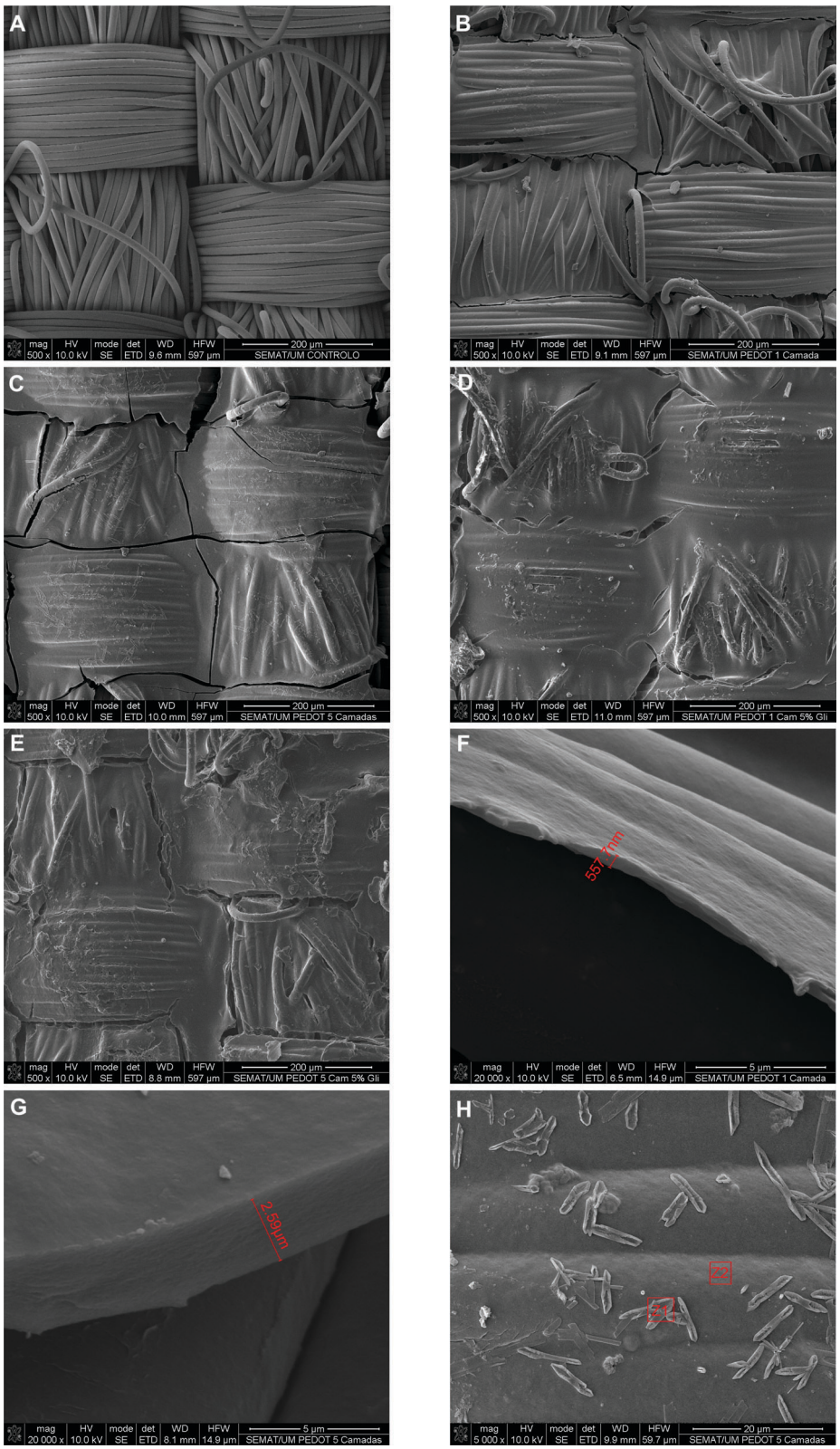

Q9 **Fig. 6** SEM images of the plasma treated polyamide 6,6 control (A); 1 layer of PEDOT:PSS (B); 5 layers of PEDOT:PSS (C); 1 layer of PEDOT:PSS + 5% w/w glycerol (D); 5 layers of PEDOT:PSS + 5% w/w glycerol (E); the thickness of 1 layer of PEDOT:PSS (F); the thickness of 5 layers of PEDOT:PSS (G); detail of the sample with 5 layers of PEDOT:PSS with the EDX analysis spots (H).

Table 3 EDS analysis of weight and atomic percentages of the sample surface with 5 layers of PEDOT:PSS (Fig. 7H)

	Z1		Z2	
Element	Wt%	At%	Wt%	At%
C	43.25	56.25	51.71	66.91
O	31.63	30.88	18.34	17.82
S	17.30	8.43	24.06	11.66
Na	4.07	2.77	3.67	2.48
Ca	2.62	1.02	0.82	0.32
Al	1.13	0.66	1.39	0.80

inversely proportional to resistance, the fabric coated with 5 layers of polymer requires a much lower voltage to reach the same temperature.[94]

The fabric coated with 5 layers of PEDOT:PSS + GLY needs only 7.5 V to induce a temperature change up to 38 °C (higher than human body core temperature), while for the 1-layer coated fabric application of at least 24 V is necessary to reach the same temperature. It is clear that the Joule heating performance of the fabrics is strongly dependent on the PEDOT:PSS layer thickness as well as the applied voltage which indicates the controllability of the electric heating performance.[95] A the steady-state temperature was achieved in the first minute of the 10 min measurement confirming a fast response time.[96] Moreover, the application of a relatively low voltage of 12 V up to 1 hour did not show any differences in temperature indicating the good stability of the system.

These results confirm the higher safety and controllability of the conducting polymers when compared to the reported metal-wire systems that typically lasted between 10–20 min at 5 V before failure due to thermal degradation of the fabric components.[97] The low applied voltages necessary for Joule heating do not pose a safety risk because the human skin resistance is in the order of 10 kΩ, much larger than that of the conductive fabrics.

Fig. 8 shows the samples placed under an infrared camera for evaluating the temperature distribution of the Joule heating effect. The images represent the temperature profile after 60 min of applied electric current of 2 A at a voltage of 12 V. The fabrics coated with 1 and 5 layer of PEDOT:PSS without glycerol did not show any increment in the contact free temperature displaying an average temperature of 19 °C in both the fabrics (Fig. 8A and B). The addition of glycerol to the PEDOT:PSS system increased the average temperature at the surface of the fabric coated with 1 layer of PEDOT:PSS from 19 to 25 °C with the appearance of hot-spot areas reaching 30 °C (Fig. 8C). When 5 layers of PEDOT:PSS + GLY were applied, the fabric reached an average temperature of 64 °C with several areas reaching a temperature above 80 °C (Fig. 8D). The general distribution of temperature did not show uniform heat generation and thermal conduction due to the non-uniformity of the PEDOT:PSS layer thicknesses on the fabric resulting in variations of the resistance.[98]

Despite the need to improve the uniformity of the PEDOT:PSS coating in the fabrics, the observed results are quite impressive since they can be compared to the temperature obtained in carbon nanotube composites using similar voltages.[99] The current irreversibly drops at voltages higher than 46 and 21 V for 1 and 5 layers of doped PEDOT:PSS, respectively. This effect can be associated both with the aging of PEDOT at high voltages and with exfoliation (Fig. S5 in ESI†) of the coating from the fibre due to high temperature.[100] This explanation is consistent with the fact that the drop in conductivity coincides with the temperature of about 100 °C achieved in both the fabrics before current disruption. The oxygen in atmospheric air and the hygroscopic nature of the polymer are probably the most important factors that promote the irreversible structural modifications (further discussion about the SEM and XRD results is available in the ESI†) of the PEDOT:PSS chains hindering the conductivity of the coating (Fig. S4 and S5 in ESI†).[101] This indicates that a suitable passivation must be provided to the PEDOT:PSS coated fabric and that high-temperature applications should be avoided.[102]

The authors are working on the application of the developed system as a heating element in a winter jacket. The design of the active clothing will be able to ensure an appropriate distribution of temperatures on the inner side of the clothing and at the same time reduce the heat dispersion on the outer

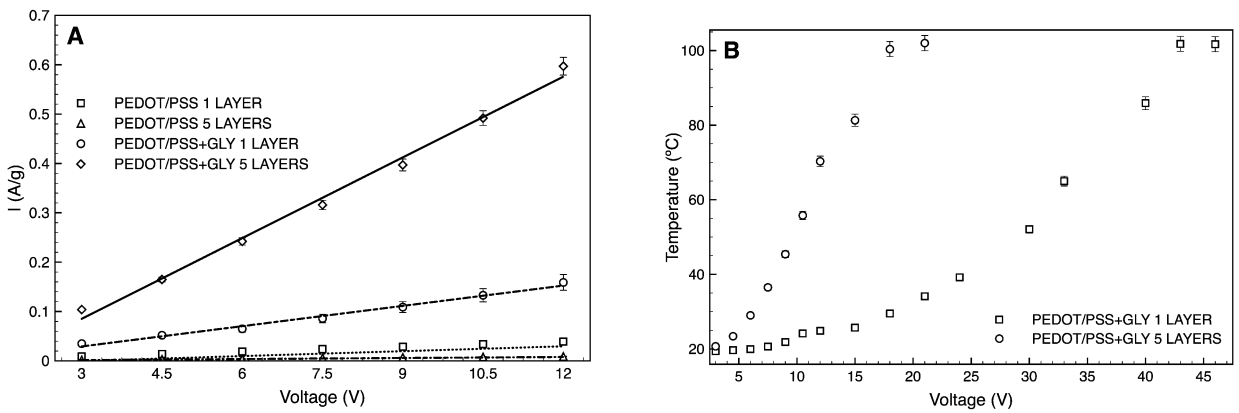

Fig. 7 current *versus* voltage (A) and temperature *versus* voltage (B) applied for 10 min of the plasma treated PA66 fabric with 1 and 5 layers of deposited PEDOT:PSS and PEDOT:PSS + 5% w/w of glycerol.

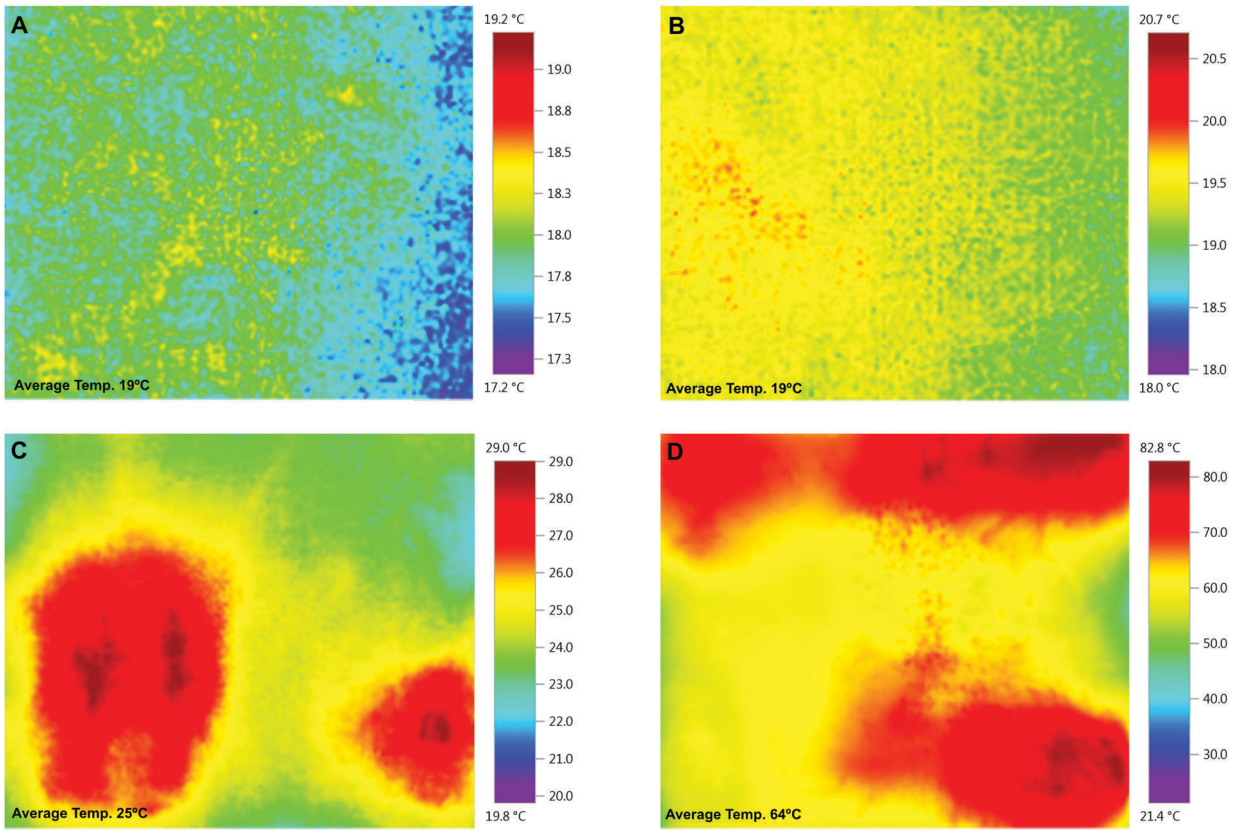

Fig. 8 Thermal images of the plasma treated PA66 fabric with 1 layer of PEDOT:PSS (A), 5 layers of PEDOT:PSS 5 layers (B), 1 layer of PEDOT:PSS + 5% w/w glycerol (C), and 5 layers of PEDOT:PSS + 5% w/w glycerol (D) after 60 min of applied voltage (12 V).

side of the clothing. The conductive fabric will be encapsulated between two different types of separators: an outer layer, that is the material between the heater and the environment and an inner layer that is the material between the heater and the skin. The outer layer will be prepared using a breathable insulating material able to reflect part of the heat generated by the conductive fabric back to the interior of the garment. In fact, it was reported that a two-fold increase in the thermal insulating power of the outer layer is able to decrease the required heating power by about 20%.[103] The inner layer will be composed of a thin breathable and water resistant material in order to promote a uniform temperature distribution and to avoid the entrance of moisture in the system. Moreover, an additional air layer will be provided between the inner layer and the skin in order to reduce the temperature by radiation and convection phenomena in the case of limited heat exchange between the layers.

Strain *versus* current

To evaluate the electrical current stability requirement for practical wearable applications, PEDOT:PSS + GLY coated fabric was tested under a tensile stress up to 250 N. Moreover, bending and torsion deformation cycles were applied in order to simulate the use of the heating element under real conditions. The obtained results can be observed in the ESI† (Fig. S10 in ESI†). The tensile test of the fabric coated with 5 layers of PEDOT:PSS with glycerol suggests that its electrical properties depend on the deformation of the textile material. With the increase of the applied force the current follows a quasi-hyperbolic decay. At the end of the test (250 N), the fabric lost 80% of its conductivity and displayed an elongation of about 4 mm. However, after 6 minutes the fabric was able to recover its conductivity exhibiting 50% of the initial current. This remarkable partial regain of current indicates that the conductive surface coating of PEDOT:PSS is not the only factor responsible for the fabric conductivity, and suggests that the conductive polymer is well spread into the fibre interior. This assumption was reinforced by another test performed until break (data not shown). The fabric partially broke at the load of 400 N and with an elongation of about 9 mm. Despite only part of the fabric and some fibres still closed the circuit also in this case the system was able to recover 50% of the initial current. It is important to highlight that a load of 10 N is a generous estimation of the maximum to be expected in a garment during normal use.[104] Thus, it is expected that the application of this heating element in a winter jacket will not cause significant loss of conductivity.

The bending and torsion tests reveal similar patterns. It can be seen from Fig. S10 (ESI†) that during the bending and twisting cycles there is a reduction of 30% and 40% in current, respectively. However, the system is able to completely recover the initial current after the solicitation was removed. All these deformation tests reveal an acceptable electromechanical

stability and flexibility of the PEDOT:PSS coating required for wearable conductive textiles.

Conclusions

The presented work shows the promising potential of this technique for creating flexible heating elements in wearable textiles with lower cost and ease of processing. The results demonstrate that the addition of glycerol leads to a structural reorientation of PEDOT:PSS chains, increasing the coating stability and conductivity (100 times increase in current density) of the blend as well decreasing the enthalpy, glass transition temperature, crystallinity and melting point of the composite fabric. The PEDOT:PSS + GLY strong interfacial adhesion to the fibres, high mechanical scratching and bending stability and also its dispersion in the bulk PA66 open up new routes for conductive flexible composite materials, which may be better than conventional metal electrodes. The resistivity, EIS and CV tests indicate that both the plasma pre-treatment and the glycerol addition induce more stability, higher resistance and capacitive performances. Moreover, they demonstrate that the Joule heating performance of the composite fabric is strongly dependent on the PEDOT:PSS + GLY layer thickness (0.5 μm for each deposited layer) as well as the applied voltage (only 7.5 V of applied voltage is needed to induce a temperature higher than the human body core temperature) confirming the higher safety and controllability of the electric heating performance. The heating element has also demonstrated its wearability being able to maintain an acceptable degree of conductivity under tension, bending and torsion deformations. A winter jacket prototype with active heating is already in the development phase. The conductive fabric will be encapsulated between an outer heat-reflecting layer and an inner thin layer able to provide uniform temperature distribution. However, more research is needed to optimise the coating process with regard to the homogeneity of the layer thickness and to the ageing of PEDOT:PSS that reduces polymer conductivity with time.

Acknowledgements

The authors acknowledge the Portuguese Foundation for Science and Technology (FCT) funding from the projects UID/EEA/04436/2013 and UID/CTM/00264/2013 and FEDER funds through the COMPETE 2020 – Programa Operacional Competitividade e Internacionalização (POCI) with the reference projects POCI-01-0145-FEDER-007136 and POCI-01-0145-FEDER-006941. EMFV is grateful for financial support through the FCT grant SFRH/BPD/95905/2013.

Notes and references

1 T. Bashir, L. Fast, M. Skrifvars and N. K. Persson, *J. Appl. Polym. Sci.*, 2012, **124**, 2954–2961.
2 T. Yamashita, S. Takamatsu, K. Miyake and T. Itoh, *Sens. Actuators, A*, 2013, **195**, 213–218.
3 M. Stoppa and A. Chiolerio, *Sensors*, 2014, **14**, 11957–11992.
4 A. Pantelopoulos and N. G. Bourbakis, *IEEE Trans. Syst., Man, Cybern., Part C: Appl. Rev.*, 2010, **40**, 1–12.
5 S. Can, A. E. Yilmaz, C. Donciu, M. Temneanu and A. S. Ardeleanu, *Tekstil Ve Konfeksiyon*, 2015, **25**, 220–228.
6 A. Tognetti, F. Lorussi, G. Mura, N. Carbonaro, M. Pacelli, R. Paradiso and D. Rossi, *J. NeuroEng. Rehabil.*, 2014, **11**, 1–17.
7 J. Lee, H. Kwon, J. Seo, S. Shin, J. H. Koo, C. Pang, S. Son, J. H. Kim, Y. H. Jang, D. E. Kim and T. Lee, *Adv. Mater.*, 2015, **27**, 2433–2439.
8 H. Zhao, L. Hou and Y. Lu, *Mater. Des.*, 2016, **95**, 97–106.
9 N. Zhang, J. Chen, Y. Huang, W. Guo, J. Yang, J. Du, X. Fan and C. Tao, *Adv. Mater.*, 2016, **28**, 263–269.
10 Z. Chai, N. Zhang, P. Sun, Y. Huang, C. Zhao, H. J. Fan, X. Fan and W. Mai, *ACS Nano*, 2016, **10**, 9201–9207.
11 L. Dong, C. Xu, Y. Li, Z.-H. Huang, F. Kang, Q.-H. Yang and X. Zhao, *J. Mater. Chem. A*, 2016, **4**, 4659–4685.
12 S. Kim, J.-S. Roh and E. Y. Lee, *Fashion Text. Res. J.*, 2016, **18**, 363–373.
13 M. D. Irwin, D. A. Roberson, R. I. Olivas, R. B. Wicker and E. MacDonald, *Fibers Polym.*, 2011, **12**, 904–910.
14 K. Jost, G. Dion and Y. Gogotsi, *J. Mater. Chem. A*, 2014, **2**, 10776–10787.
15 M. Akerfeldt, M. Straat and P. Walkenstrom, *Text. Res. J.*, 2012, **83**, 618–627.
16 H. Miura, Y. Fukuyama, T. Sunda, B. J. Lin, J. Zhou, J. Takizawa, A. Ohmori and M. Kimura, *Adv. Eng. Mater.*, 2014, **16**, 550–555.
17 H. K. Kim, M. S. Kim, S. Y. Chun, Y. H. Park, B. S. Jeon, J. Y. Lee, Y. K. Hong, J. Joo and S. H. Kim, *Mol. Cryst. Liq. Cryst.*, 2003, **405**, 161–169.
18 S. Seyedin, J. M. Razal, P. C. Innis, A. Jeiranikhameneh, S. Beirne and G. G. Wallace, *ACS Appl. Mater. Interfaces*, 2015, **7**, 21150–21158.
19 Y. Ding, M. A. Invernale and G. A. Sotzing, *ACS Appl. Mater. Interfaces*, 2010, **2**, 1588–1593.
20 T. Bashir, M. Ali, S.-W. Cho, N.-K. Persson and M. Skrifvars, *Polym. Adv. Technol.*, 2013, **24**, 210–219.
21 G. G. Wallace, T. E. Campbell and P. C. Innis, *Fibers Polym.*, 2007, **8**, 135–142.
22 Y.-J. Lin, W.-S. Ni and J.-Y. Lee, *J. Appl. Phys.*, 2015, **117**, 215501.
23 A. G. Obukhov, S. Tsukada, H. Nakashima and K. Torimitsu, *PLoS One*, 2012, **7**, e33689.
24 T. Bashir, M. Skrifvars and N.-K. Persson, *Polym. Adv. Technol.*, 2012, **23**, 611–617.
25 M. Akerfeldt, M. Straat and P. Walkenstrom, *Text. Res. J.*, 2013, **83**, 2164–2176.
26 D. Knittel and E. Schollmeyer, *Synth. Met.*, 2009, **159**, 1433–1437.
27 K. Opwis, D. Knittel and J. S. Gutmann, *Synth. Met.*, 2012, **162**, 1912–1918.
28 J. Ouyang and Y. Yang, *Adv. Mater.*, 2006, **18**, 2141–2144.
29 S. Zhang, P. Kumar, A. S. Nouas, L. Fontaine, H. Tang and F. Cicoira, *APL Mater.*, 2015, **3**, 014911.

30 P. C. Khandelwal, S. S. Agrawal, M. A. G. Namboothiry and N. Gundiah, *J. Mater. Chem. B*, 2014, **2**, 7327–7333.

31 M. Vosgueritchian, D. J. Lipomi and Z. Bao, *Adv. Funct. Mater.*, 2012, **22**, 421–428.

32 L. Ouyang, C. Musumeci, M. J. Jafari, T. Ederth and O. Inganäs, *ACS Appl. Mater. Interfaces*, 2015, **7**, 19764–19773.

33 W. H. Kim, G. P. Kushto, H. Kim and Z. H. Kafafi, *J. Polym. Sci., Part B: Polym. Phys.*, 2003, **41**, 2522–2528.

34 S. Hamdani, P. Potluri and A. Fernando, *Materials*, 2013, **6**, 1072–1089.

35 V. Koncar, Assoc, C. Cochrane, M. Lewandowski, F. Boussu and C. Dufour, *Int. J. Clothing Sci. Technol.*, 2009, **21**, 82–92.

36 W. Więźlak and J. Zieliński, *Int. J. Clothing Sci. Technol.*, 1993, **5**, 9–23.

37 O. Bubnova, Z. U. Khan, A. Malti, S. Braun, M. Fahlman, M. Berggren and X. Crispin, *Nat. Mater.*, 2011, **10**, 429–433.

38 J. Zhou, M. Mulle, Y. Zhang, X. Xu, E. Q. Li, F. Han, S. T. Thoroddsen and G. Lubineau, *J. Mater. Chem. C*, 2016, **4**, 1238–1249.

39 J. Charles, G. R. Ramkumaar, S. Azhagiri and S. Gunasekaran, *E-J. Chem.*, 2009, **6**, 23–33.

40 K. H. Kale and S. S. Palaskar, *J. Text. Inst.*, 2012, **103**, 1088–1098.

41 D. J. Upadhyay, N. Y. Cui, C. A. Anderson and N. M. D. Brown, *Colloids Surf., A*, 2004, **248**, 47–56.

42 C. Menchaca, A. Alvarez-Castillo, G. Martinez-Barrera, H. Lopez-Valdivia, H. Carrasco and V. M. Castano, *Int. J. Mater. Prod. Technol.*, 2003, **19**, 521–529.

43 S. Xu, Y. Luo, G. Liu, G. Qiao, W. Zhong, Z. Xiao, Y. Luo and H. Ou, *Electrochim. Acta*, 2015, **156**, 20–28.

44 B. Friedel, P. E. Keivanidis, T. J. K. Brenner, A. Abrusci, C. R. McNeill, R. H. Friend and N. C. Greenham, *Macromolecules*, 2009, **42**, 6741–6747.

45 T. P. Nguyen, P. Le Rendu, P. D. Long and S. A. De Vos, *Surf. Coat. Technol.*, 2004, **180–181**, 646–649.

46 W. H. Kim, G. P. Kushto, H. Kim and Z. H. Kafafi, *J. Polym. Sci., Part B: Polym. Phys.*, 2003, **41**, 2522–2528.

47 B. D. Martin, N. Nikolov, S. K. Pollack, A. Saprigin, R. Shashidhar, F. Zhang and P. A. Heiney, *Synth. Met.*, 2004, **142**, 187–193.

48 H. J. Snaith, H. Kenrick, M. Chiesa and R. H. Friend, *Polymer*, 2005, **46**, 2573–2578.

49 H.-E. Yin, C.-H. Wu, K.-S. Kuo, W.-Y. Chiu and H.-J. Tai, *J. Mater. Chem.*, 2012, **22**, 3800–3810.

50 F. Denes, *Prog. Polym. Sci.*, 2004, **29**, 815–885.

51 E. C. Botelho, N. Scherbakoff, M. C. Rezende, A. M. Kawamoto and J. Sciamareli, *Macromolecules*, 2001, **34**, 3367–3375.

52 L. Quintanilla, J. C. Rodriguezcabello and J. M. Pastor, *Polymer*, 1994, **35**, 2321–2328.

53 F. Navarro-Pardo, G. Martínez-Barrera, A. Martínez-Hernández, V. Castaño, J. Rivera-Armenta, F. Medellín-Rodríguez and C. Velasco-Santos, *Materials*, 2013, **6**, 3494–3513.

54 G. Z. Zhang, T. Watanabe, H. Yoshida and T. Kawai, *Polym. J.*, 2003, **35**, 173–177.

55 G. Zhang, T. Watanabe, H. Yoshida and T. Kawai, *Polym. J.*, 2003, **35**, 173–177.

56 Y. Li, X. Zhu, G. Tian, D. Yan and E. Zhou, *Polym. Int.*, 2001, **50**, 677–682.

57 C. Caamaño, B. Grady and D. E. Resasco, *Carbon*, 2012, **50**, 3694–3707.

58 L. Yow-Jon, N. Wei-Shih and L. Jhe-You, *J. Appl. Phys.*, 2015, **117**, 215501.

59 M. H. Rahimi, M. Parvinzadeh, M. Y. Navid and S. Ahmadi, *J. Surfactants Deterg.*, 2011, **14**, 595–603.

60 S. El-Sayed, K. H. Mahmoud, A. A. Fatah and A. Hassen, *Physica B*, 2011, **406**, 4068–4076.

61 R. Sengupta, S. Sabharwal, A. K. Bhowmick and T. K. Chaki, *Polym. Degrad. Stab.*, 2006, **91**, 1311–1318.

62 C. J. Lee and I. S. Tsai, *Mater. Sci. Forum*, 2011, **687**, 625–633.

63 A. Gómez-Siurana, A. Marcilla, M. Beltrán, D. Berenguer, I. Martínez-Castellanos and S. Menargues, *Thermochim. Acta*, 2013, **573**, 146–157.

64 K. F. Babu, T. N. Narayanan and M. A. Kulandainathan, *Adv. Mater. Interfaces*, 2014, **1**, 1300139.

65 J. Zhou, D. H. Anjum, L. Chen, X. Xu, I. A. Ventura, L. Jiang and G. Lubineau, *J. Mater. Chem. C*, 2014, **2**, 9903–9910.

66 A. Patole, I. A. Ventura and G. Lubineau, *J. Appl. Polym. Sci.*, 2015, **132**, 42281.

67 J. Zhou and M. Kimura, *Sen-I Gakkaishi*, 2011, **67**, 125–131.

68 J. Zhou, I. Aguilar Ventura and G. Lubineau, *Ind. Eng. Chem. Res.*, 2014, **53**, 3539–3549.

69 U. Lang, N. Naujoks and J. Dual, *Synth. Met.*, 2009, **159**, 473–479.

70 E. Corradini, S. H. Imam, J. A. M. Agnelli and L. H. C. Mattoso, *J. Polym. Environ.*, 2009, **17**, 1–9.

71 M. Lavorgna, F. Piscitelli, P. Mangiacapra and G. G. Buonocore, *Carbohydr. Polym.*, 2010, **82**, 291–298.

72 S. P. Luo, J. Z. Cao and Y. Peng, *Polym. Compos.*, 2014, **35**, 201–207.

73 A. Zille, M. M. Fernandes, A. Francesko, T. Tzanov, M. Fernandes, F. R. Oliveira, L. Almeida, T. Amorim, N. Carneiro, M. F. Esteves and A. P. Souto, *ACS Appl. Mater. Interfaces*, 2015, **7**, 13731–13744.

74 W. Wang, M. A. Ruderer, E. Metwalli, S. Guo, E. M. Herzig, J. Perlich and P. Müller-Buschbaum, *ACS Appl. Mater. Interfaces*, 2015, **7**, 8789–8797.

75 M.-W. Lee, M.-Y. Lee, J.-C. Choi, J.-S. Park and C.-K. Song, *Org. Electron.*, 2010, **11**, 854–859.

76 J. Jian, X. Guo, L. Lin, Q. Cai, J. Cheng and J. Li, *Sens. Actuators, B*, 2013, **178**, 279–288.

77 T. J. Whitcher, N. A. Talik, K. Woon, N. Chanlek, H. Nakajima, T. Saisopa and P. Songsiriritthigul, *J. Phys. D: Appl. Phys.*, 2014, **47**, 055109.

78 , *J. Appl. Phys.*, 2015, **117**, 215501.

79 D. J. Lipomi, J. A. Lee, M. Vosgueritchian, B. C. K. Tee, J. A. Bolander and Z. Bao, *Chem. Mater.*, 2012, **24**, 373–382.

80 A. Zille, F. R. Oliveira and A. P. Souto, *Plasma Processes Polym.*, 2015, **12**, 98–131.

81 F. R. Oliveira, A. Zille and A. P. Souto, *Appl. Surf. Sci.*, 2014, **293**, 177–186.

82 R. Dorai and M. J. Kushner, *J. Phys. D: Appl. Phys.*, 2003, **36**, 666–685.
83 S. R. S. Prabaharan, R. Vimala and Z. Zainal, *J. Power Sources*, 2006, **161**, 730–736.
84 Y. Hou, Y. W. Cheng, T. Hobson and J. Liu, *Nano Lett.*, 2010, **10**, 2727–2733.
85 B. B. Yue, C. Y. Wang, X. Ding and G. G. Wallace, *Electrochim. Acta*, 2012, **68**, 18–24.
86 G. Yu, L. Hu, M. Vosgueritchian, H. Wang, X. Xie, J. R. McDonough, X. Cui, Y. Cui and Z. Bao, *Nano Lett.*, 2011, **11**, 2905–2911.
87 J. Molina, A. L. del Rio, J. Bonastre and F. Cases, *Eur. Polym. J.*, 2009, **45**, 1302–1315.
88 P. R. Roberge, *Handbook of corrosion engineering*, McGraw-Hill, New York, 2nd edn, 2012.
89 N. K. Vu, A. Zille, F. R. Oliveira, N. Carneiro and A. P. Souto, *Plasma Processes Polym.*, 2013, **10**, 285–296.
90 D. Schaubroeck, J. De Smet, W. Willems, P. Cools, N. De Geyter, R. Morent, H. De Smet and G. Van Steenbeerge, *Appl. Surf. Sci.*, 2016, **376**, 151–160.
91 T. Takano, H. Masunaga, A. Fujiwara, H. Okuzaki and T. Sasaki, *Macromolecules*, 2012, **45**, 3859–3865.
92 Q. Wei, M. Mukaida, Y. Naitoh and T. Ishida, *Adv. Mater.*, 2013, **25**, 2831–2836.
93 J. Ouyang, Q. Xu, C.-W. Chu, Y. Yang, G. Li and J. Shinar, *Polymer*, 2004, **45**, 8443–8450.
94 P.-C. Hsu, X. Liu, C. Liu, X. Xie, H. R. Lee, A. J. Welch, T. Zhao and Y. Cui, *Nano Lett.*, 2015, **15**, 365–371.
95 J. Yan and Y. G. Jeong, *Mater. Des.*, 2015, **86**, 72–79.
96 Y. Atwa, N. Maheshwari and I. A. Goldthorpe, *J. Mater. Chem. C*, 2015, **3**, 3908–3912.
97 T. M. Schweizer, *M.S. thesis*, Georgia Institute of Technology, 2005.
98 J. Zhou, T. Fukawa, H. Shirai and M. Kimura, *Macromol. Mater. Eng.*, 2010, **295**, 671–675.
99 A. Laforgue, G. Rouget, S. Dubost, M. F. Champagne and L. Robitaille, *ACS Appl. Mater. Interfaces*, 2012, **4**, 3163–3168.
100 H. Okuzaki and M. Ishihara, *Macromol. Rapid Commun.*, 2003, **24**, 261–264.
101 E. Vitoratos, S. Sakkopoulos, N. Paliatsas, K. Emmanouil and S. A. Choulis, *Open J. Org. Polym. Mater.*, 2012, **02**, 7–11.
102 I. W. Kwon, H. J. Son, W. Y. Kim, Y. S. Lee and H. C. Lee, *Synth. Met.*, 2009, **159**, 1174–1177.
103 W. Więźlak and J. Zieliński, *Int. J. Clothing Sci. Technol.*, 1993, **5**, 9–23.
104 R. J. Bassett, R. Postle and N. Pan, *Text. Res. J.*, 1999, **69**, 866–875.